doi:10.1038/nature10636

Two ten-billion-solar-mass black holes at the centres of giant elliptical galaxies

Nicholas J. McConnell[1], Chung-Pei Ma[1], Karl Gebhardt[2], Shelley A. Wright[1], Jeremy D. Murphy[2], Tod R. Lauer[3], James R. Graham[1,4] & Douglas O. Richstone[5]

Observational work conducted over the past few decades indicates that all massive galaxies have supermassive black holes at their centres. Although the luminosities and brightness fluctuations of quasars in the early Universe suggest that some were powered by black holes with masses greater than 10 billion solar masses[1,2], the remnants of these objects have not been found in the nearby Universe. The giant elliptical galaxy Messier 87 hosts the hitherto most massive known black hole, which has a mass of 6.3 billion solar masses[3,4]. Here we report that NGC 3842, the brightest galaxy in a cluster at a distance from Earth of 98 megaparsecs, has a central black hole with a mass of 9.7 billion solar masses, and that a black hole of comparable or greater mass is present in NGC 4889, the brightest galaxy in the Coma cluster (at a distance of 103 megaparsecs). These two black holes are significantly more massive than predicted by linearly extrapolating the widely used correlations between black-hole mass and the stellar velocity dispersion or bulge luminosity of the host galaxy[5–9]. Although these correlations remain useful for predicting black-hole masses in less massive elliptical galaxies, our measurements suggest that different evolutionary processes influence the growth of the largest galaxies and their black holes.

Empirical scaling relations between black-hole mass (M_{BH}), galaxy bulge velocity dispersion (σ) and luminosity (L) are commonly used to estimate black-hole masses, because for most galaxies we are unable to make a direct measurement. Estimates of the number density of black holes in a given mass range thus depend upon the empirically determined M_{BH}–σ and M_{BH}–L relations over an appropriate range of galaxy masses. Directly measuring M_{BH} from the kinematics of stars or gas in the vicinity of the black hole is particularly difficult at the highest galaxy masses, because massive galaxies are rare, their typical distances from Earth are large and their central stellar densities are relatively low. The most massive galaxies are typically brightest cluster galaxies (BCGs), that is, giant elliptical galaxies that reside near the centres of galaxy clusters.

We have obtained high-resolution, two-dimensional data of the line-of-sight stellar velocities in the central regions of NGC 3842 and NGC 4889 using integral-field spectrographs at the Gemini North and Keck 2 telescopes, in Hawaii. The stellar luminosity distribution of each galaxy is provided by surface photometry from NASA's Hubble Space Telescope and ground-based telescopes[10,11]. NGC 3842 is the BCG of Abell 1367, a moderately rich galaxy cluster. NGC 4889 is the BCG of the Coma cluster (Abell 1656), one of the richest nearby galaxy clusters. We targeted these two galaxies because they have relatively high central surface brightnesses and lie at an accessible distance for direct measurements of M_{BH}.

We measured the distribution of stellar velocities at 82 different locations in NGC 3842. The line-of-sight velocity dispersion in NGC 3842 is between 270 and 300 km s^{-1} at large galactocentric radii (r) and rises in the central 0.7 arcsec ($r < 330$ pc), peaking at 326 km s^{-1} (Figs 1 and 2). We determined the mass of the central black hole by constructing a series of orbit superposition models[12]. Each model assumes a black-hole mass, stellar mass-to-light ratio and dark-matter profile, and generates a library of time-averaged stellar orbits in the resulting gravitational potential. The model then fits a weighted combination of orbital line-of-sight velocities to the set of measured stellar velocity distributions. The goodness-of-fit statistic χ^2 is computed as a function of the assumed values of M_{BH} and the stellar mass-to-light ratio. Using our best-fitting model dark-matter halo, we measure a black-hole mass of 9.7×10^9 solar masses ($M_\odot$), with a 68% confidence interval of $(7.2–12.7) \times 10^9 M_\odot$. Models with no black hole are ruled out at the 99.996% confidence level ($\Delta\chi^2 = 17.1$). We find the stellar mass-to-light ratio to equal $5.1 M_\odot/L_\odot$ in the R band ($L_\odot$, solar luminosity), with a 68% confidence interval of 4.4–$5.8 M_\odot/L_\odot$.

We measured stellar velocity distributions at 63 locations in NGC 4889 and combined our measurements with published long-slit kinematics at larger radii[13]. The largest velocity dispersions in NGC 4889 are located across an extended region on the east side of the galaxy. The stellar orbits in our models are defined to be symmetric about the galaxy centre, so we constrain M_{BH} by running separate trials with velocity profiles from four quadrants of the galaxy. The best-fitting black-hole masses from the four quadrants range from $9.8 \times 10^9 M_\odot$ to $2.7 \times 10^{10} M_\odot$. All quadrants favour tangential orbits near the galaxy centre, which cause the line-of-sight velocity dispersion to decrease even as the internal three-dimensional velocity dispersion increases towards the black hole. Although no single model is consistent with all of the observed kinematic features in NGC 4889, we can define a confidence interval for M_{BH} by considering the most extreme confidence limits from the cumulative set of models. The corresponding 68% confidence interval is $(0.6–3.7) \times 10^{10} M_\odot$. We adopt a black-hole mass of $2.1 \times 10^{10} M_\odot$, corresponding to the midpoint of this interval.

Figure 3 shows the M_{BH}–σ and M_{BH}–L relations, using data compiled from studies published before the end of August 2011, plus our measurements of NGC 3842 and NGC 4889. Tabulated data with references are provided as Supplementary Information. The most widely used form for both relations is a power law with a constant exponent. Straight lines in Fig. 3 show our fits to $M_{BH}(\sigma)$ and $M_{BH}(L)$. The relationship between σ and L, however, flattens at high galaxy masses, and constant-exponent power laws for the M_{BH}–σ and M_{BH}–L relations produce contradictory predictions for M_{BH} in this mass range[14]. Direct measurements of M_{BH} in higher mass galaxies will compel the revision of one or both of the M_{BH}–σ and M_{BH}–L relations.

The average velocity dispersion in NGC 3842 is 270 km s^{-1}, measured outside the black hole radius of influence (1.2 arcsec or 570 pc) and inside the two-dimensional half-light radius (38 arcsec or 18 kpc). Although NGC 3842 hosts a black hole more massive than any previously detected, its average dispersion ranks only fourteenth

[1]Department of Astronomy, University of California, Berkeley, California 94720, USA. [2]Department of Astronomy, University of Texas, Austin, Texas 78712, USA. [3]National Optical Astronomy Observatory, Tucson, Arizona 85726, USA. [4]Dunlap Institute for Astronomy and Astrophysics, University of Toronto, Ontario M5S 3H4, Canada. [5]Department of Astronomy, University of Michigan, Ann Arbor, Michigan 48109, USA.

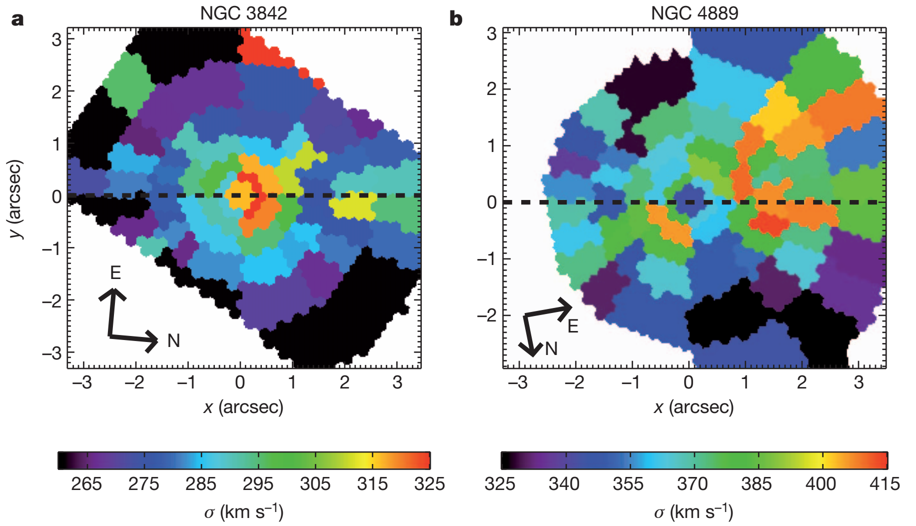

Figure 1 | Two-dimensional maps of the line-of-sight stellar velocity dispersions. The maps show the central regions of NGC 3842 (**a**) and NGC 4889 (**b**) observed using the GMOS spectrograph[23] on the 8-m Gemini North telescope. Additional kinematics at large radii were measured using the VIRUS-P spectrograph[24] on the 2.7-m Harlan J. Smith telescope, and additional high-resolution data were acquired with OSIRIS spectrograph[25] at the 10-m Keck 2 telescope. GMOS, OSIRIS and VIRUS-P are all integral-field spectrographs, which record spectra at multiple positions in a two-dimensional spatial array. The horizontal dashed line in each panel traces the major axis of the galaxy. The median 1-s.d. errors in velocity dispersion are 12 km s^{-1} and 20 km s^{-1} for NGC 3842 and NGC 4889, respectively. In NGC 4889, the highest velocity dispersions, near 410 km s^{-1}, are located on the east side of the galaxy, at least 1.1 arcsec from the centre.

among 65 galaxies with direct measurements of $M_{\rm BH}$. Its luminosity ranks fifth in this sample of galaxies and is exceeded only by other BCGs. On the basis of the values of σ and L for NGC 3842, our revised $M_{\rm BH}$–σ and $M_{\rm BH}$–L relations predict that $M_{\rm BH} = 9.1 \times 10^8 M_\odot$ and $2.5 \times 10^9 M_\odot$, respectively. Similarly, for NGC 4889 the respective predictions are $M_{\rm BH} = 3.3 \times 10^9 M_\odot$ and $4.5 \times 10^9 M_\odot$. These predictions are smaller than our direct measurements of $M_{\rm BH}$ by 1.6–4.6 times the 1-s.d. scatter in the $M_{\rm BH}$–σ and $M_{\rm BH}$–L relations[9]. Four measurements of $M_{\rm BH}$ in BCGs existed before this work. Two measurements based on gas dynamics and one based on stellar dynamics all lie within 1.2 s.d. of our revised fits to the $M_{\rm BH}$–σ and $M_{\rm BH}$–L relations[15,16]. Yet the measurement of $M_{\rm BH}$ in NGC 1316, the BCG of the Fornax cluster, is 3.4 s.d. less than that predicted by our $M_{\rm BH}$–L relation[17]. The high scatter indicated by this collection of measurements reveals large uncertainties in the standard practice of using galactic σ or L as a proxy for the central black-hole mass in giant elliptical galaxies and their predecessors.

Several BCGs within 200 Mpc of Earth are at least twice as luminous as NGC 3842 and three times as luminous as Messier 87, which hosted the most massive black hole known before this work. In spite of their extreme luminosities, BCGs have velocity dispersions similar to those of the most massive field elliptical galaxies. Yet the most massive black holes are found predominantly in BCGs (Fig. 3). How galaxies are assembled and the role of gas dissipation affect the correlations (or lack thereof) among $M_{\rm BH}$, σ and L. Simulations of mergers of gas-rich disk galaxies are able to produce remnant galaxies that follow the observed $M_{\rm BH}$–σ correlation in Fig. 3a over the intermediate mass range $M_{\rm BH} \approx 10^7 M_\odot$–$10^9 M_\odot$ (refs 18, 19). By contrast, simulated mergers of elliptical galaxies with low-angular-momentum progenitor orbits increase $M_{\rm BH}$ and L by similar numerical factors, without increasing the velocity dispersion[20]. Because these mergers are a likely path to forming the most massive galaxies, the $M_{\rm BH}$–σ correlation may steepen or disappear altogether at the highest galaxy masses. Massive elliptical galaxies retain residual quantities of gas even after the decline of star formation. Accretion of this gas onto the galaxies' central black

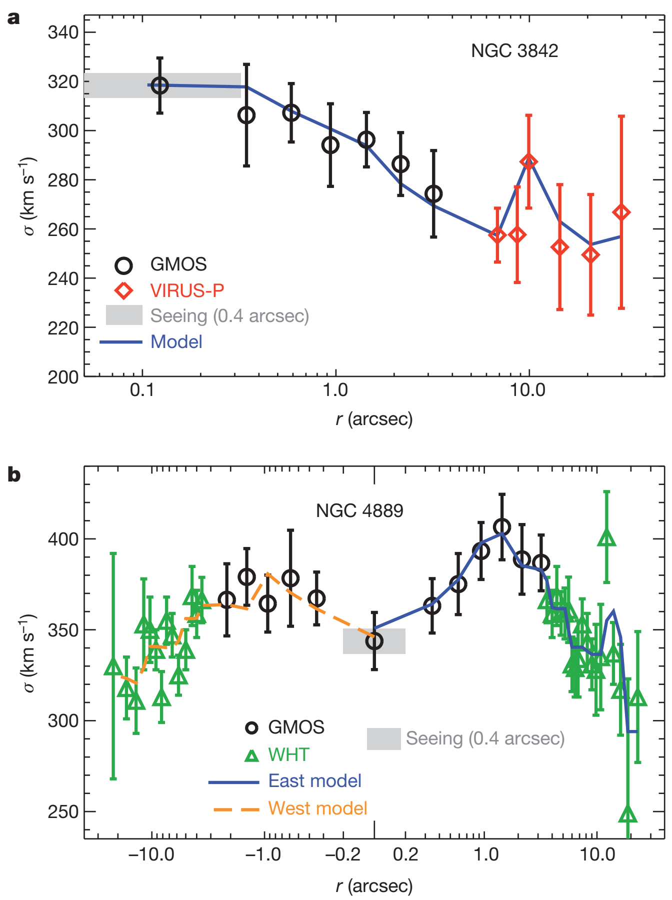

Figure 2 | One-dimensional profiles of the line-of-sight velocity dispersions. **a**, Dispersion versus radius in NGC 3842, after averaging data at a given radius, based on measurements with GMOS (black circles) and VIRUS-P (red diamonds). The solid blue line is the projected line-of-sight dispersion from our best-fitting stellar orbit model of NGC 3842. **b**, Dispersion versus radius along the major axis of NGC 4889, measured using GMOS (black circles) and the William Herschel Telescope[13] (WHT; green triangles). The maximum velocity dispersion occurs at $r = 1.4$ arcsec. The solid blue line is the projected line-of-sight dispersion from our best-fitting orbit model using data from the east side of NGC 4889 ($r > 0$). The dashed orange line is from our best-fitting orbit model using data from the west side of NGC 4889 ($r < 0$). Error bars, 1 s.d.

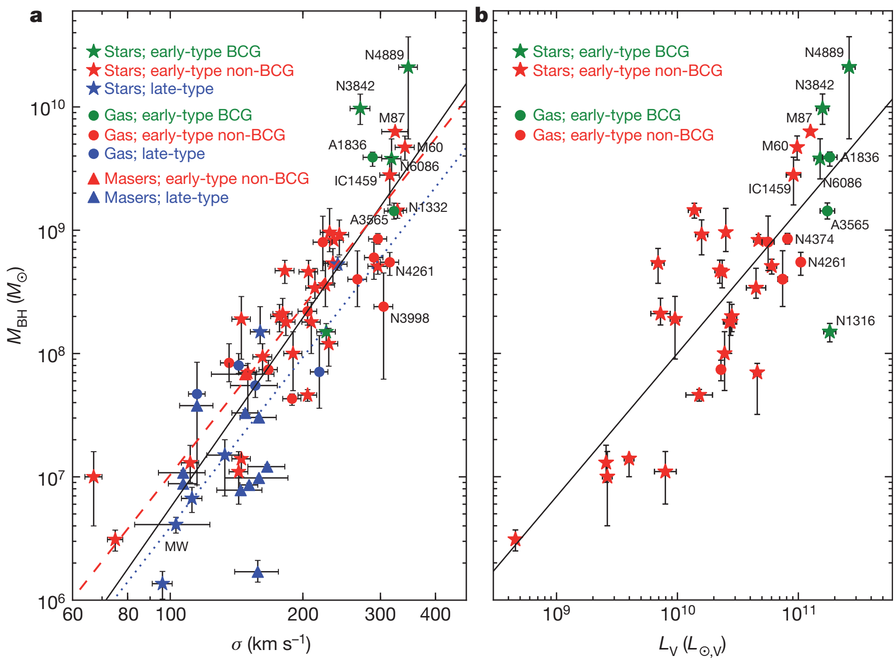

Figure 3 | Correlations of dynamically measured black hole masses and bulk properties of host galaxies. **a**, Black-hole mass (M_{BH}) versus stellar velocity dispersion (σ) for 65 galaxies with direct dynamical measurements of M_{BH}. For galaxies with spatially resolved stellar kinematics, σ is the luminosity-weighted average within one effective radius (Supplementary Information). **b**, Black-hole mass versus V-band bulge luminosity, L_V ($L_{\odot,V}$, solar value), for 36 early-type galaxies with direct dynamical measurements of M_{BH}. Our sample of 65 galaxies consists of 32 measurements from a 2009 compilation[9], 16 galaxies with masses updated since 2009, 15 new galaxies with M_{BH} measurements and the two galaxies reported here. A complete list of the galaxies is given in Supplementary Table 4. BCGs (defined here as the most luminous galaxy in a cluster) are plotted in green, other elliptical and S0 galaxies are plotted in red, and late-type spiral galaxies are plotted in blue. The black-hole masses are measured using the dynamics of masers (triangles), stars (stars) or gas (circles). Error bars, 68% confidence intervals. For most of the maser galaxies, the error bars in M_{BH} are smaller than the plotted symbol. The solid black line in **a** shows the best-fitting power law for the entire sample: $\log_{10}(M_{BH}/M_\odot) = 8.29 + 5.12\log_{10}[\sigma/(200\,\mathrm{km\,s^{-1}})]$. When early-type and late-type galaxies are fitted separately, the resulting power laws are $\log_{10}(M_{BH}/M_\odot) = 8.38 + 4.53\log_{10}[\sigma/(200\,\mathrm{km\,s^{-1}})]$ for elliptical and S0 galaxies (dashed red line) and $\log_{10}(M_{BH}/M_\odot) = 7.97 + 4.58\log_{10}[\sigma/(200\,\mathrm{km\,s^{-1}})]$ for spiral galaxies (dotted blue line). The solid black line in **b** shows the best-fitting power law: $\log_{10}(M_{BH}/M_\odot) = 9.16 + 1.16\log_{10}(L_V/10^{11}L_\odot)$. We do not label Messier 87 as a BCG, as is commonly done, because NGC 4472 in the Virgo cluster is 0.2 mag brighter.

holes could help increase M_{BH} and further steepen the M_{BH}–σ and M_{BH}–L relations.

Black holes in excess of $10^{10}M_\odot$ are observed as quasars in the early Universe, from 1.4×10^9 to 3.3×10^9 yr after the Big Bang[2] (redshift, $z = 2$–4.5). Throughout the last 1.0×10^{10} yr, however, these extremely massive black holes have not been accreting appreciably, and the average mass of the black holes powering quasars has decreased steadily. Quasar activity and elliptical galaxy formation are predicted to arise from similar merger-triggered processes, and there is growing evidence that present-day massive elliptical galaxies once hosted the most-luminous high-redshift quasars[21]. However, definitive classification of these quasars' host galaxies has remained elusive.

Our measurements of black holes with masses of around $10^{10}M_\odot$ in NGC 3842 and NGC 4889 provide circumstantial evidence that BCGs host the remnants of extremely luminous quasars. The number density of nearby BCGs ($\sim5\times10^{-6}\,\mathrm{Mpc^{-3}}$) is consistent with the number density of black holes ($\sim3\times10^{-7}$ to $10^{-5}\,\mathrm{Mpc^{-3}}$) with masses between $10^9M_\odot$ and $10^{10}M_\odot$ predicted from the M_{BH}–L relation and the luminosity function of nearby galaxies. Furthermore, both quantities agree with predictions based on the black-hole masses and duty cycles of quasars. The black-hole number density predicted from the M_{BH}–σ relation, however, is an order of magnitude less than the inferred quasar population[14,22]. These two predictions can be reconciled if the M_{BH}–σ relation has upward curvature or a large degree of intrinsic scatter in M_{BH} at the high-mass end, as suggested by our new measurements. With improvements in adaptive optics instrumentation on large optical telescopes and very-long-baseline interferometry at radio wavelengths, black holes are being sought and detected in increasingly exotic host galaxies. Along with our measurements of the black-hole masses in NGC 3842 and NGC 4889, future measurements in other massive galaxies will quantify the cumulative growth of supermassive black holes in the Universe's densest environments.

Received 15 July; accepted 13 October 2011.

1. Netzer, H. The largest black holes and the most luminous galaxies. *Astrophys. J.* **583,** L5–L8 (2003).
2. Vestergaard, H., Fan, X., Tremonti, C. A., Osmer, P. S. & Richards, G. T. Mass functions of the active black holes in distant quasars from the Sloan Digital Sky Survey data release 3. *Astrophys. J.* **674,** L1–L4 (2008).
3. Sargent, W. L. W. *et al.* Dynamical evidence for a central mass concentration in the galaxy M87. *Astrophys. J.* **221,** 731–744 (1978).
4. Gebhardt, K. *et al.* The black hole mass in M87 from Gemini/NIFS adaptive optics observations. *Astrophys. J.* **729,** 119 (2011).
5. Dressler, A. in *Active Galactic Nuclei* (eds Osterbrock, D. E. & Miller, J. S.) 217–232 (IAU Symposium 134, Springer, 1989).
6. Kormendy, J. & Richstone, D. Inward bound the search for supermassive black holes in galactic nuclei. *Annu. Rev. Astron. Astrophys.* **33,** 581–624 (1995).
7. Ferrarese, L. & Merritt, D. A fundamental relation between supermassive black holes and their host galaxies. *Astrophys. J.* **539,** L9–L12 (2000).
8. Gebhardt, K. *et al.* A relationship between nuclear black hole mass and galaxy velocity dispersion. *Astrophys. J.* **539,** L13–L16 (2000).
9. Gültekin, K. *et al.* The $M_{BH}-\sigma$ and $M_{BH}-L$ relations in galactic bulges, and determinations of their intrinsic scatter. *Astrophys. J.* **698,** 198–221 (2009).
10. Laine, S. *et al.* Hubble Space Telescope imaging of brightest cluster galaxies. *Astron. J.* **125,** 478–505 (2003).
11. Postman, M. & Lauer, T. R. Brightest cluster galaxies as standard candles. *Astrophys. J.* **440,** 28–47 (1995).
12. Schwarzschild, M. A numerical model for a triaxial stellar system in dynamical equilibrium. *Astrophys. J.* **232,** 236–247 (1979).
13. Loubser, S. I., Sansom, A. E., Sánchez-Blázquez, P., Soechting, I. K. & Bromage, G. E. Radial kinematics of brightest cluster galaxies. *Mon. Not. R. Astron. Soc.* **391,** 1009–1028 (2008).
14. Lauer, T. R. *et al.* The masses of nuclear black holes in luminous elliptical galaxies and implications for the space density of the most massive black holes. *Astrophys. J.* **662,** 808–834 (2007).

15. Dalla Bontà, E. *et al.* The high-mass end of the black hole mass function: mass estimates in brightest cluster galaxies. *Astrophys. J.* **690,** 537–559 (2009).
16. McConnell, N. J. *et al.* The black hole mass in brightest cluster galaxy NGC 6086. *Astrophys. J.* **728,** 100 (2011).
17. Nowak, N. *et al.* The supermassive black hole of Fornax A. *Mon. Not. R. Astron. Soc.* **391,** 1629–1649 (2008).
18. Di Matteo, T., Volker, S. & Hernquist, L. Energy input from quasars regulates the growth and activity of black holes and their host galaxies. *Nature* **433,** 604–607 (2005).
19. Robertson, B. *et al.* The evolution of the $M_{BH} - \sigma$ relation. *Astrophys. J.* **641,** 90–102 (2006).
20. Boylan-Kolchin, M., Ma, C.-P. & Quataert, E. Red mergers and the assembly of massive elliptical galaxies: the fundamental plane and its projections. *Mon. Not. R. Astron. Soc.* **369,** 1081–1089 (2006).
21. Hopkins, P. F., Bundy, K., Hernquist, L. & Ellis, R. S. Observational evidence for the coevolution of galaxy mergers, quasars, and the blue/red galaxy transition. *Astrophys. J.* **659,** 976–996 (2007).
22. Lauer, T. R., Tremaine, S., Richstone, D. & Faber, S. M. Selection bias in observing the cosmological evolution of the $M_{BH}-\sigma$ and $M_{BH}-L$ relationships. *Astrophys. J.* **670,** 249–260 (2007).
23. Allington-Smith, J. *et al.* Integral field spectroscopy with the Gemini Multi-Object Spectrograph. I. Design, construction, and testing. *Publ. Astron. Soc. Pacif.* **114,** 892–912 (2002).
24. Hill, G. J. *et al.* Design, construction, and performance of VIRUS-P: the prototype of a highly replicated integral field spectrograph for the HET. *Proc. Soc. Photo-opt. Instrum. Eng.* **7014,** 701470 (2008).
25. Larkin, J. *et al.* OSIRIS: a diffraction limited integral field spectrograph for Keck. *Proc. Soc. Photo-opt. Instrum. Eng.* **6269,** 62691A (2006).

Supplementary Information is linked to the online version of the paper at www.nature.com/nature.

Acknowledgements N.J.M., C.-P.M, K.G. and J.R.G. are supported by the National Science Foundation. C.-P.M. is supported by NASA and by the Miller Institute for Basic Research in Science, University of California, Berkeley. S.A.W. is supported by NASA through a Hubble Fellowship. Data presented here were obtained using the Gemini Observatory, the W. M. Keck Observatory and the McDonald Observatory. The Gemini Observatory is operated by the Association of Universities for Research in Astronomy, Inc., under a cooperative agreement with the National Science Foundation on behalf of the Gemini partnership. The W. M. Keck Observatory is operated as a scientific partnership among the California Institute of Technology, the University of California and NASA. The McDonald Observatory is operated by the University of Texas at Austin. The instrument VIRUS-P was funded by G. and C. Mitchell. Stellar orbit models were run using the facilities at the Texas Advanced Computing Center at The University of Texas at Austin.

Author Contributions N.J.M. carried out the data analysis and modelling. N.J.M, C.-P.M. and S.A.W. wrote the manuscript. C.-P.M. compiled the data for Fig. 3 and oversaw communication among co-authors. S.A.W. analysed OSIRIS data on NGC 3842. K.G. provided GMOS data on NGC 3842 and NGC 4889. K.G. and D.O.R. developed the stellar orbit modelling code. J.D.M. provided VIRUS-P data on NGC 3842. T.R.L. provided photometric data on and image analysis of NGC 3842 and NGC 4889. J.R.G. led the OSIRIS observing campaign for NGC 3842. All authors contributed to the interpretive analysis of the observations and the writing of the paper.

Author Information Reprints and permissions information is available at www.nature.com/reprints. The authors declare no competing financial interests. Readers are welcome to comment on the online version of this article at www.nature.com/nature. Correspondence and requests for materials should be addressed to N.J.M. (nmcc@berkeley.edu) or C.-P.M. (cpma@berkeley.edu).